Photoinduced recharging process of Ni_{Ga} in GaP and paramagnetic resonance of Ni_{Ga}^{2+}

1991 J. Phys.: Condens. Matter 3 6345

(http://iopscience.iop.org/0953-8984/3/33/013)

J. Phys.: Condens. Matter 3 (1991) 6345–6362. Printed in the UK

Photoinduced recharging processes of Ni_{Ga} in GaP and paramagnetic resonance of Ni^{2+}_{Ga}

A Erramli†, M S G Al-Ahmadi‡§, W Ulrici‖, N Tebbal†, J Kreissl¶, A-M Vasson†, A Vasson† and C A Bates‡

† LPMC Physique 4, URA CNRS No 796, Université Blaise Pascal–Clermont Ferrand II, 63177 Aubière Cédex, France

‡ Physics Department, University of Nottingham, Nottingham NG7 2RD, UK

‖ Zentralinstitut für Elektronenphysik, Hausvogteiplatz 5–7, 1086 Berlin, Federal Republic of Germany

¶ Zentrum für Wissenschaftlichen Gerätebau, Rudower Chaussee 6, 1199 Berlin, Federal Republic of Germany

Received 22 January 1991, in final form 18 April 1991

Abstract. LEC-grown GaP:Ni in which the Fermi level is pinned by either the Ni^{2+}/Ni^{3+} or Ni^{+}/Ni^{2+} level has been investigated by optical absorption (OA), thermally detected (TD) optical absorption, electron paramagnetic resonance (EPR) and TD-EPR. The spectroscopic features, subsequently assigned to Ni^{+}_{Ga}, Ni^{2+}_{Ga} and Ni^{3+}_{Ga}, were monitored under external illumination. The analysis of their spectral dependence together with the angular variation of a set of new TD-EPR peaks strongly suggests that the latter results are due to Ni^{2+}_{Ga} ions. It also provides identification of the photoinduced recharging processes involving the three charge states of isolated Ni_{Ga}. An orthorhombic Jahn–Teller model is presented to describe the Ni^{2+}_{Ga} resonances in the TD-EPR experiments.

1. Introduction

The nickel impurity in GaP has been investigated during the last two decades by several methods so that some reliable information is available [1]. In GaP, Ni acts as a double acceptor, as in GaAs. The first acceptor level $Ni^{2+}_{Ga}/Ni^{3+}_{Ga}$ has been unequivocally identified and located at $E_v + 0.51$ eV by combined DLTS and photo-EPR experiments [2] confirming an earlier result derived from Hall effect measurements [3]. The second acceptor level Ni^{+}_{Ga}/Ni^{2+}_{Ga} was found by DLTS and transient capacitance measurements at $E_c - 0.82$ eV [4] in accordance with the analysis of photocapacitance experiments [5].

Therefore, Ni_{Ga} has been investigated spectroscopically in three charge states, namely the neutral $Ni^{3+}_{Ga}(3d^7)$ state as well as in the charged $Ni^{2+}_{Ga}(3d^8)$ and $Ni^{+}_{Ga}(3d^9)$ states.

As the ground state of Ni^{3+}_{Ga} is an orbital singlet $^4A_2$, an intense EPR signal due to the $-\frac{1}{2} \rightarrow +\frac{1}{2}$ transition is observed at $g = 2.098$. For B along $\langle 100 \rangle$, a ligand hyperfine splitting of this signal arising from the interaction with the nuclear spin

§ Present address: Department of Physics, Faculty of Science, King Abdulaziz University, Jeddah, Saudi Arabia.

0953-8984/91/336345+18$03.50

on the four ^{31}P ligands [6] is resolved. Detailed ENDOR investigations made on this signal have given unequivocal proof for the spin S to be equal to $\frac{3}{2}$ and that the Ni^{3+} is located on a Ga-site in an undisturbed environment (i.e. it is isolated Ni^{3+}_{Ga}) [7]. Surprisingly, the internal transitions of Ni^{3+}_{Ga} ($^4A_2 \leftrightarrow {}^4T_2, {}^4T_1$) have not yet been detected by either optical absorption (OA) or photoluminescence (PL).

Several OA bands have been found in GaP:Ni attributed to internal transitions of Ni^{2+}_{Ga} [8–10]. The most pronounced of these is centred at about 1.25 eV with a zero-phonon line (ZPL) at 1.232 eV. It is interpreted to be due to the $^3T_1(F) \rightarrow {}^3T_1(P)$ transition. From uniaxial stress and Zeeman experiments on this ZPL, a $T \otimes e$ Jahn–Teller coupling of the $^3T_1(P)$ state has been deduced assuming that the $^3T_1(F)$ ground state is split by spin–orbit coupling [9]. From their linear correlation with the intensity of the 1.232 eV ZPL in samples with different Ni^{2+} content, a line at 0.852 eV was assigned to the $^3T_1(F) \rightarrow {}^3T_2(F)$ transition and the line at 1.41 eV to the $^3T_1(F) \rightarrow {}^1T_2(^1G)$ transition [10].

No EPR signal due to Ni^{2+}_{Ga} has been reported to date for either GaP or GaAs. However, a pronounced phonon-scattering resonance at 500 GHz was found in thermal conductivity experiments on GaP samples containing Ni^{2+}_{Ga} [11]. This resonance is attributed to the transition between the T_1 ground vibronic state and the T_2 inversion level (sometimes referred to as the tunnelling level) associated with a dynamic orthorhombic $T \otimes (e + t_2)$ Jahn–Teller effect operating within the $^3T_1(F)$ ground state. This is analogous to that attributed to the 300 GHz resonance of Ni^{2+}_{Ga} in GaAs and reported in detail by Challis *et al* [12].

The Ni^{+}_{Ga} impurity in GaP gives rise to a characteristic and intense ZPL at 0.6636 eV in both OA and PL. It has been assigned to the $\Gamma_7(^2T_2) \leftrightarrow \Gamma_8(^2E)$ transition of the $3d^9$ configuration for Ni^+ [13]. This assignment was confirmed by Zeeman [13] and uniaxial stress experiments [14] on this ZPL. The isotropic EPR signal ($\Delta B = 25$ mT) found at $g = 0.934$ is consistent with the Zeeman data obtained for the $\Gamma_7(^2T_2)$ ground state and therefore attributed to Ni^{+}_{Ga} [13]. The double acceptor Ni^{+}_{Ga} has a strong affinity with donors forming nearest-neighbour (donor on P-site) or next-nearest-neighbour (donor on Ga-site) complexes. Each complex causes a ZPL with an energy which is characteristic of the chemical nature of the donor atom in the complex and was detected by both OA and PL [15]. These results strongly support the conclusion that the ZPL at 0.6636 eV is due to isolated Ni^{+}_{Ga}.

As both acceptor levels are located within the gap, optically induced rechargings between the three charge states of Ni_{Ga} due to photoionization transitions can be expected at low temperatures depending on the Fermi level position. A first set of experiments on Ni-diffused GaP with He–Ne laser illumination ($h\nu = 1.96$ eV) has shown such rechargings from the observation of the change of intensity of the ZPLs of Ni^{+}_{Ga} and Ni^{2+}_{Ga} OA spectra and of the Ni^{3+}_{Ga} EPR signal [16].

In the present paper we investigate GaP:Ni with different Fermi level positions. The aim initially is to clarify the photoinduced recharging processes which change the relative amounts of Ni^+, Ni^{2+} and Ni^{3+}. (We use the term 'photoinduced recharging' to refer to the change of the charge state of a defect by illumination with light at temperatures low enough to prevent thermally activated recharging.) For this purpose we investigate the dependence of the characteristic spectroscopic features (e.g. absorption due to internal d–d transitions, band-to-defect transitions, or the reverse, or EPR transitions) of the three charge states on illumination energy $h\nu_{exc}$ and monitor the change in the OA, thermally detected optical absorption (TD-OA), EPR and TD-EPR experiments. A comparison of these spectral dependencies (intensities of the signal

as a function of $h\nu_{exc}$) with the photoionization cross sections $\sigma_n^o(h\nu)$ and $\sigma_p^o(h\nu)$ of both acceptor levels enables us to identify the optical excitation processes. The monitoring of the dependence of such features on the size of the quantum $h\nu_{exc}$ can give information on how the relative concentrations of a defect in a certain charge state change under illumination.

As the analysis of the phonon-scattering experiments suggests a strong coupling to the $^3T_1(F)$ ground state of Ni_{Ga}^{2+} [11, 12], TD-EPR is the most sensitive experiment in which the Ni_{Ga}^{2+} ion within the $^3T_1$ ground state can be detected. As we observe new Ni-related resonances in TD-EPR, which appear to be very sensitive to strain, we intend to verify their assignment to Ni_{Ga}^{2+} by using the previously mentioned monitoring of the photoinduced recharging of Ni_{Ga}. Finally, the behaviour of these newly detected Ni_{Ga}^{2+} resonances will be analysed by a theoretical model in which a strong orthorhombic $T_1 \otimes (e + t_2)$ Jahn–Teller effect is present.

2. Experimental methods

The Ni-doped GaP samples investigated here were taken from two boules grown by the LEC technique in a high-pressure puller. Their dimensions are 40 mm in diameter and a length of about 100 mm. The first boule (PI 1497) was doped by adding metallic nickel ($\approx$ 1 mg Ni/g GaP) to the melt. This boule was a p-type semi-insulating sample and contained at the tail end (E1 samples) about 4.2×10^{16} cm^{-3} Ni. Its Fermi level was pinned by the Ni^{2+}/Ni^{3+} level at $E_v + 0.51$ eV. The second boule (PI 1813) was also doped by adding metallic nickel and co-doped by adding Ga_2S_3 to the melt to achieve n-type Ni-doped GaP with its Fermi level located in the upper half of the gap. At the tail end (E1 samples) this GaP:Ni:S boule contains about 3×10^{16} cm^{-3} Ni and is slightly n-conducting with its Fermi level pinned at low temperatures by the S_P donor level ($E_c - 0.107$ eV). The middle part (M1 samples) of the GaP:Ni:S boule is n-type semi-insulating with its Fermi level pinned by the Ni^+/Ni^{2+} level at $E_c - 0.9$ eV ([Ni] $\sim 1.4 \times 10^{16}$ cm^{-3}).

The samples for the different experiments were cut from the E1 and M1 slices (6 mm thick) mentioned previously. Rectangular samples of size 6 mm × 7 mm × 15 mm with the large faces polished to optical quality were used for the OA and TD-OA measurements. For the EPR and TD-EPR experiments, oriented samples were used with dimensions 12 mm × 3 mm × 3 mm and 15 mm × 6 mm × 7 mm with the long axis along ⟨110⟩ or along ⟨100⟩ and polished faces to investigate the photoinduced changes of the resonance signals.

The conventional OA and EPR measurements have been carried out using a double-beam prism spectrometer and homodyne X-band ERS 230 spectrometer. In both TD-OA and TD-EPR, the temperature rise of the signal as a result of the phonon emission, due to non-radiative de-excitation or relaxation, is detected via a carbon glass thermometer at liquid helium temperatures [17, 18].

3. Experimental results

3.1. p-type GaP:Ni

We have investigated in detail the E1 samples of the GaP:Ni boule (PI 1497). Curve 1 of figure 1 shows the OA spectrum at $T = 78$ K after cooling down in the dark. It

consists of the two absorption bands due to the $^3T_1(F) \rightarrow {}^3T_2$ (0.9 eV) and $\rightarrow {}^3T_1(P)$ (1.25 eV) transitions of Ni^{2+}_{Ga} [10] and of two broad intense photoionization absorptions with onsets at approximately 1.4 and 1.85 eV. The TD-OA spectrum obtained at $T = 1.7$ K (figure 2, curve 1) shows the structure of the $\rightarrow {}^3T_1(P)$ absorption in more detail with the ZPL at 1.232 eV and the weak lines around 1.41 eV assigned to the $\rightarrow {}^1T_2$ transition of Ni^{2+}_{Ga}. A TD-OA signal is also observed at 0.852 eV ($^3T_1(F) \rightarrow {}^3T_2(F)$ of Ni^{2+}_{Ga}). Furthermore, an unidentified line at 0.723 eV is seen by TD-OA. Such a line has been previously reported for GaP:Ni [8]. In the EPR spectra measured at $T = 20$ K in the dark, the isotropic resonance ($g = 2.089$) due to Ni^{3+}_{Ga} [6] can be detected, even though it is weak, in addition to the five-line spectrum due to Fe^{3+}_{Ga} as the samples contain unintentional Fe as a residual impurity. These results clearly indicate that, in the GaP:Ni E1 samples, the Fermi level is pinned by the Ni^{2+}/Ni^{3+} acceptor level as features of both Ni^{2+} and Ni^{3+} could be identified in the dark. However, most of the nickel is in the Ni^{2+} state.

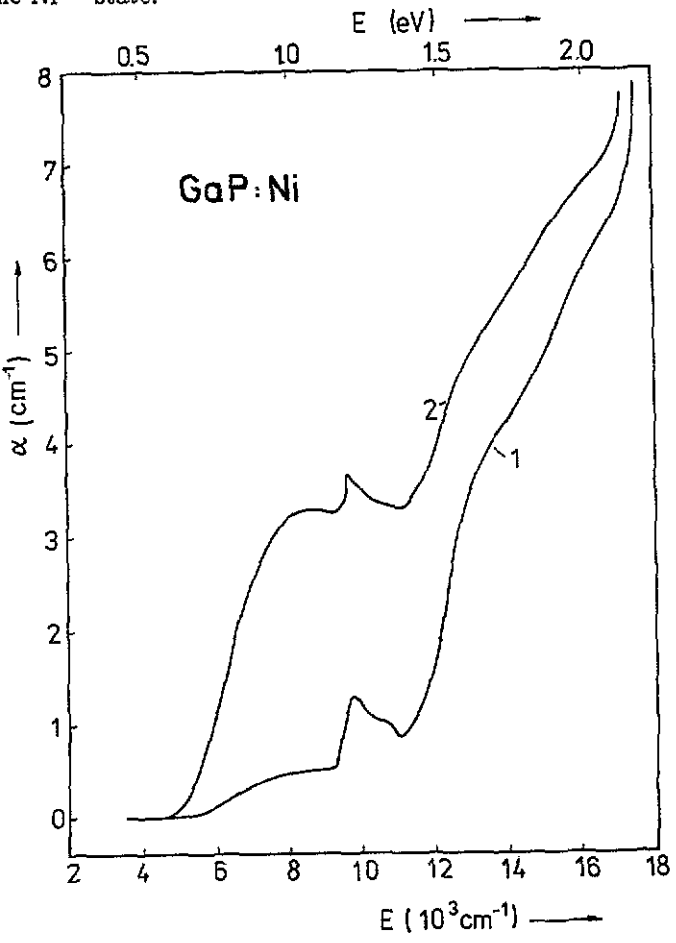

Figure 1. Optical absorption spectra of GaP:Ni (boule PI 1497, sample E1) at $T = 78$ K: curve 1, after cooling down in the dark; curve 2, after illumination with light of $h\nu_{exc} = 2.0$ eV.

Figure 3 shows the TD-EPR spectra for magnetic fields $0.2 < B < 0.8$ T with B parallel to the three main crystallographic directions. In addition to the signal at

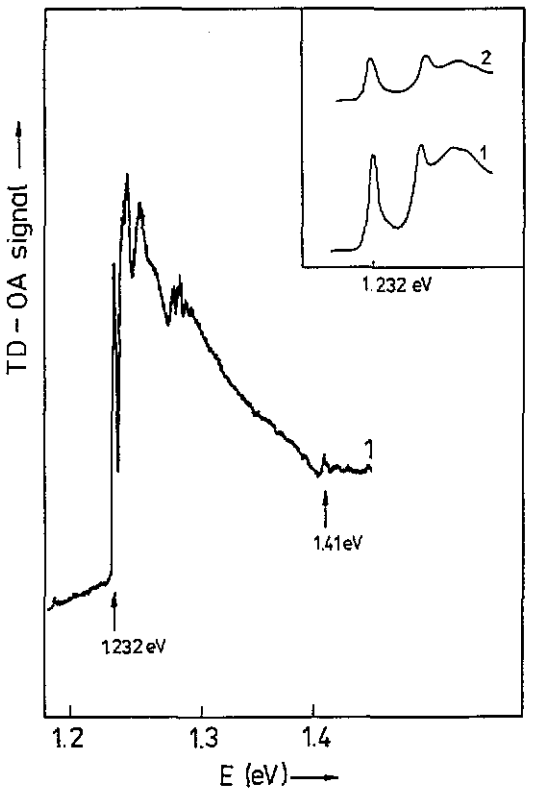

Figure 2. TD-OA spectra of GaP:Ni (boule PI 1497, sample E1) measured at $T = 1.7$ K in the region of the $^3T_1 \rightarrow {}^3T_1(P)$ transition of Ni^{2+}_{Ga} with the ZPL at 1.232 eV. Curve 1 is measured after cooling down in the dark. The weak structure at 1.41 eV has been assigned to the $\rightarrow {}^1T_2({}^1G)$ transition of Ni^{2+}_{Ga} [10]. The inset with an expanded energy scale shows the ZPL after cooling in the dark (1) and after illumination with light of $h\nu_{exc} = 1.6$ eV (2).

$g = 2.09$, which is dominated by the Ni^{3+}_{Ga} resonance, new lines can be seen (marked by Δ). They are also detectable before illumination. They should be due to Ni-centres and will be provisionally labelled as Ni^{n+} lines. This assignment to Ni seems to be justified as Ni is the dopant and its content is much larger than that of residual paramagnetic impurities. Furthermore, these Ni^{n+} lines have never been found in the TD-EPR spectra of GaP doped with other transition metals (Ti, V, Cr, Mn, Fe, Co).

Curve 2 in figure 1 shows the OA spectrum after illumination using radiation of energy $h\nu_{exc} = 2.0$ eV. A new broad photoionization band appears with onset at approximately 0.55 eV and a maximum at approximately 1.08 eV. This absorption is assigned to the photoionization transition:

$$Ni^{3+}_{Ga} + h\nu_{exc} \rightarrow Ni^{2+}_{Ga} + hole_{vb} \qquad (1)$$

and is caused by the photoinduced creation of Ni^{3+}_{Ga}. Simultaneously, the intensity of the band for the transition to the $^3T_1(P)$ level and of both photoionization absorptions, with onset at 1.4 and 1.85 eV, are decreased. A linear correlation is found between the increase in the Ni^{3+}/Ni^{2+} absorption (1) and the decrease in the $\rightarrow {}^3T_1(P)$ band of Ni^{2+}. The spectral dependence of the photoinduced Ni^{3+} absorption (1) is shown in figure 4 together with the photoinduced decrease of the intensity of the $^3T_1(F)$

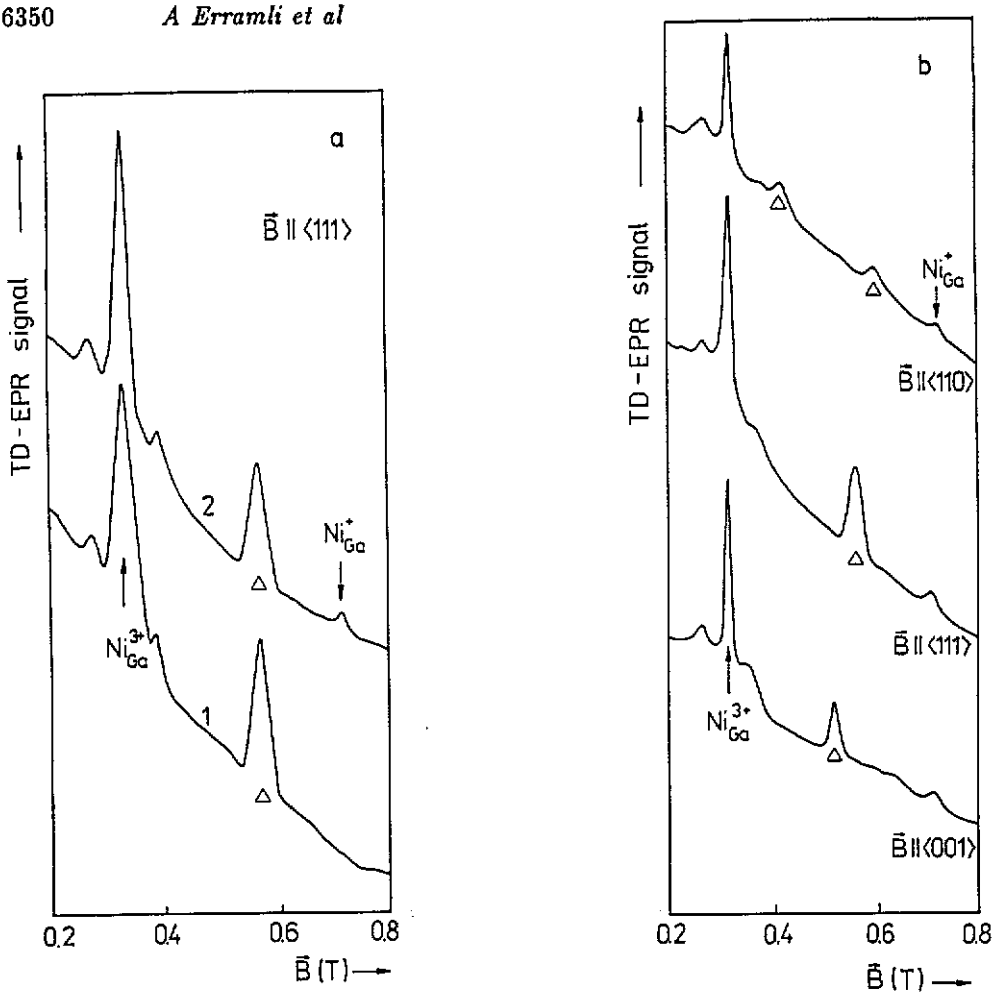

Figure 3. Thermally detected EPR spectra of GaP:Ni (PI 1497, E1) measured at $T = 4$ K, with $\nu = 9.3$ GHz for B along (a) ⟨111⟩ and (b) ⟨001⟩, ⟨111⟩ and ⟨110⟩: curve 1, after illumination with light of energy $h\nu_{exc} = 1.55$ eV; curve 2, and the curves in (b) after illumination with light of $h\nu_{exc} = 2.06$ eV. The triangles mark the Ni^{2+} resonance lines.

$\rightarrow {}^3T_1(P)$ absorption of Ni^{2+}_{Ga}. This has been monitored by measuring the dependence on $h\nu_{exc}$ of the TD-OA spectrum, (see figure 2). The relative intensity of the ZPL at 1.232 eV is given in figure 4. All data points given in figure 4 (and also those in figures 5, 9 and 10) are taken after illumination with $h\nu_{exc}$ where the signal intensity is normalized to that of the highest one measured. To a good approximation, they correspond to the steady state values during the illumination as the decay in the dark is very slow (as noted later). The steady state values of the signals depend only very weakly on the illumination intensity due to the experimental arrangement (150 W tungsten lamp combined with metal interference filters and Si or GaAs edge filters).

Similar photoinduced experiments were also carried out by EPR and TD-EPR. Curve 2 in figures 3(a) and 3(b) show the TD-EPR spectra measured after illumination with $h\nu_{exc} = 2.06$ eV. The important photoinduced changes are the increase in the Ni^{3+}_{Ga} signal at $g = 2.089$, the appearance of an isotropic signal at $g = 0.934$ which can be unambiguously assigned to Ni^{+}_{Ga} [13], and the decrease in the Ni^{n+} lines for $h\nu_{exc}$

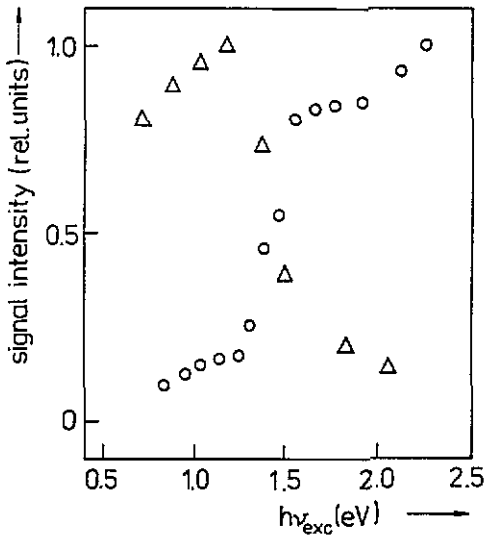

Figure 4. Dependence of the photoinduced changes on illumination energy $h\nu_{exc}$ of GaP:Ni (cf figures 1 and 2): open circles, Ni^{3+}/Ni^{2+} photoionization absorption (1) measured at 1.0 eV and $T = 78$ K; open triangles, intensity of the ZPL at 1.232 eV of the $\rightarrow {}^3T_1(P)$ transition of Ni^{2+}_{Ga} measured by TD-OA at $T = 1.7$ K.

larger than 1.4 eV. The Ni^{3+}_{Ga} signal measured by conventional EPR also increases under illumination. It should be emphasized that the Ni^{3+}_{Ga} EPR signal with its characteristically resolved phosphorus hyperfine interaction (five lines) for B along ⟨100⟩ is indeed due to isolated Ni_{Ga} as has been proved by ENDOR experiments on this signal [6]. All these photoinduced changes of the intensities of the resonance signal have been measured as functions of the energy $h\nu_{exc}$ of the illuminating light. The spectral dependencies are shown in figure 5.

Although the absolute concentrations of the Ni-charge states could be determined in some experiments (even with large errors), it is impossible to do so in other experiments particularly in TD-OA, C-EPR and in TD-EPR. This arises because, in these measurements, either the random strain distribution function or the ion–lattice coupling constants or both are involved explicitly in determining the intensity. However, these values are not needed to fulfil the aims of this paper; the qualitative information needed can be obtained from the normalized change in the signal intensity as a function of $h\nu_{exc}$. That is, we correlate the increases or decreases in intensities which occur at the onsets.

The most important correlations suggested by figures 4 and 5 are:

(i) there is a large increase in Ni^{3+} for $h\nu_{exc} > 1.4$ eV with a second weaker step at $h\nu_{exc} \approx 1.85$ eV in all spectra obtained from OA, EPR and TD-EPR;

(ii) the same spectral dependence as found with Ni^{3+} is found for the TD-EPR Ni^{+}_{Ga} signal; and

(iii) the spectral dependencies of the Ni^{2+}_{Ga} ZPL intensity and of the Ni^{n+} TD-EPR signal intensity are similar; there is a strong decrease in both for $h\nu_{exc} > 1.2$ eV which is the region where the Ni^{3+} and Ni^{+} signals increase.

It should be mentioned that the weak increase in Ni^{3+} for $0.8 < h\nu_{exc} < 1.4$ eV is accompanied by a sharp decrease in the Fe^{3+}_{Ga} EPR signal intensity.

The photoinduced rechargings discussed earlier decay only very slowly in the dark

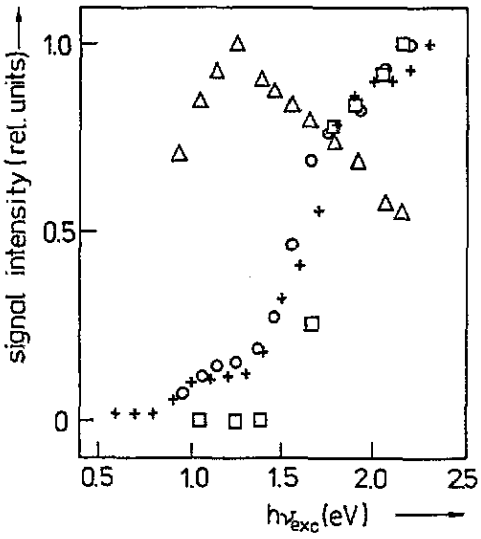

Figure 5. Dependence of the photoinduced changes on illumination energy $h\nu_{exc}$ of GaP:Ni (cf figure 3). The TD-EPR signal intensities measured at $T = 4$ K for B along ⟨111⟩: open circles, Ni^{3+}_{Ga}; open squares, Ni^{+}_{Ga}; open triangles, Ni^{2+}. The conventional EPR signal (+) of Ni^{3+}_{Ga} is measured at $T = 20$ K.

at $T < 120$ K after switching off the illumination; the decay varies as $-\ln(t/\tau)$ with $\tau \simeq 10^8$–10^{10} s. However, the original situation can be restored optically by illumination with light of energy $0.55 < h\nu_b < 1.4$ eV, i.e. by illumination into the Ni^{3+}/Ni^{2+} photoionization band according to (1). This is illustrated in figure 6.

3.2. n-type GaP:Ni:S

Samples from the middle part (M1) of GaP:Ni:S (boule PII 1813) have been investigated in the same comprehensive manner as those described in section 3.1 because, in these n-type M1 samples, the Fermi level is well defined in the upper half of the gap. As can be seen from the TD-OA spectra given in figures 7 and 8, both the Ni^{+}_{Ga} (with its ZPL at 0.6636 meV characteristic for isolated Ni^{+}_{Ga}) and Ni^{2+}_{Ga} absorptions are clearly visible where most of the Ni seems to be in the Ni^{2+} state in the dark.

The TD-EPR spectra of the M1 samples obtained at $T = 4$ K in the dark show the resonance due to Ni^{+}_{Ga} as well as those labelled as Ni^{n+}.

Once more it is apparent that illumination causes a light-energy-dependent change of the intensity of the different signals due to photoinduced recharging. The spectral dependencies of the TD-OA signals due to Ni^{2+}_{Ga} and Ni^{+}_{Ga} are given in figure 9. Figure 10 shows these dependencies for the Ni^{+}_{Ga} and the Ni^{n+} TD-EPR signals and, for $h\nu_{exc} > 1.4$ eV, the resonance due to Ni^{3+}_{Ga} which appears in both TD-EPR and EPR. The appearance and increase of Ni^{3+} for $h\nu_{exc} > 1.4$ eV could also be detected in the OA and TD-OA spectra at $T = 78$ K by the absorption according to (1).

From figures 9 and 10, the following correlations can be clearly derived:

(i) the Ni^{+}_{Ga} signals measured by TD-OA and TD-EPR and present in the dark increase with an onset at $h\nu_{exc} \approx 1.4$ eV;

(ii) the Ni^{3+}_{Ga} signals measured by EPR and TD-EPR, absent in the dark, appear at $h\nu_{exc} \approx 1.4$ eV; and

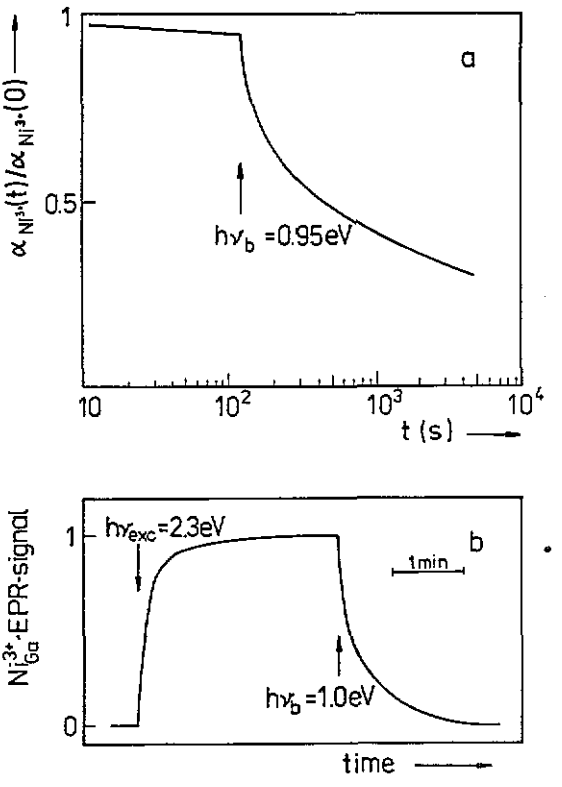

Figure 6. Time dependence of the photoinduced recharging in GaP:Ni. (*a*) Decay of the photoinduced Ni^{3+} absorption measured at $T = 78$ K in the dark after switching off $h\nu_{exc} = 2.0$ eV at $t = 0$; at $t = 120$ s, the bleaching illumination $h\nu_b$ is switched on resulting in a drastic decay. (*b*) Increase and decay of the Ni^{3+}_{Ga} EPR signal measured at $T = 20$ K.

(iii) the spectral dependence of the Ni^{2+}_{Ga} TD-OA signal (e.g. ZPL at 1.232 eV) and of the Ni^{n+} TD-EPR signal are again nearly identical with the onset of their decrease at $h\nu_{exc} \approx 1.4$ eV.

The photoinduced rechargings are also, in the M1 sample of GaP:Ni:S, very stable in the dark at $T < 120$ K but can be restored optically with light 0.55 eV $< h\nu_b <$ 1.4 eV in an analogous manner to that described for GaP:Ni E1 in section 3.1.

The results discussed earlier confirm that, in the GaP:Ni:S M1 samples, the Fermi level is pinned by the Ni^+/Ni^{2+} level at about $E_c - 0.9$ eV as the features of both charge states are detectable in the dark. This is supported by the absence of the Fe^+_{Ga} resonance signal (i.e. the Fe^+_{Ga}/Fe^{2+}_{Ga} level at $E_c - 0.26$ eV is empty). Moreover, for $h\nu_{exc} > 1.4$ eV the EPR signal due to Fe^{3+}_{Ga} appears and the spectral dependence of its intensity coincides with that of Ni^{3+}_{Ga} as shown in figure 10.

4. Interpretation

4.1. Identification of the paramagnetic resonances due to Ni^{2+}_{Ga}

The Ni^{n+} resonances detected by TD-EPR occur in both p-type GaP:Ni E1 with Ni^{2+} and Ni^{3+} present and in n-type GaP:Ni:S M1 where Ni^{2+} and Ni^+ are the charge

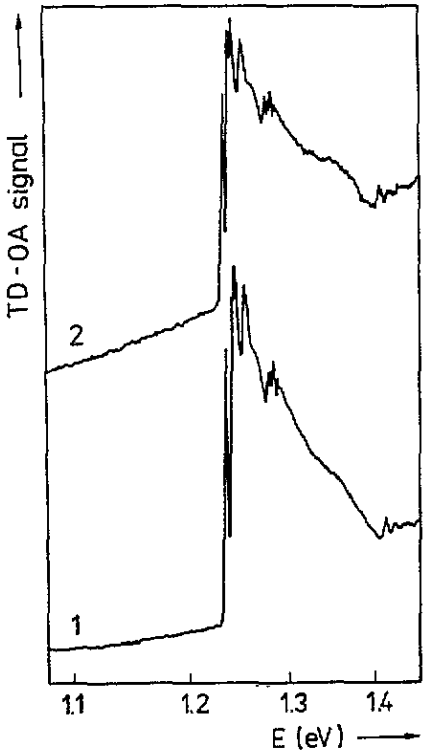

Figure 7. The TD-OA spectra of GaP:Ni:S (sample M1) measured at $T = 1.7$ K in the region of the $^3T_1(F) \rightarrow {}^3T_1(P)$ transition of Ni^{2+}_{Ga}: curve 1, after cooling in the dark; curve 2, after illumination with $h\nu_{exc} = 1.6$ eV.

states of nickel on a gallium site. In both types of sample, the spectral dependence of the photoinduced change of the Ni^{n+} resonances is similar to that of the optically detected Ni^{2+}_{Ga} features† as can be seen in figures 4, 5, 9 and 10. Therefore, these results suggest that the Ni^{n+} resonances can be due to Ni^{2+}_{Ga}.

The interpretation of different photoinduced recharging processes involving the three charge states of Ni_{Ga} given in the following section will confirm this conclusion.

4.2. Photoinduced recharging processes

As already mentioned in section 3.1, in the p-type GaP:Ni E1 samples the Fermi level is pinned at $E_v + 0.51$ eV. This means that the Ni^{2+}/Ni^{3+} level is partly filled (both charge states are present) and the Ni^{+}/Ni^{2+} level at $E_c - 0.9$ eV is empty. Therefore, besides transition (1) the following photoionization processes are possible (see also figure 11):

$$Ni^{2+}_{Ga} + h\nu \rightarrow Ni^{+}_{Ga} + hole_{vb} \tag{2}$$

$$Ni^{2+}_{GA} + h\nu \rightarrow Ni^{3+}_{Ga} + e_{cb} \tag{3}$$

where the onset of (2) is expected at $h\nu \approx 1.4$ eV and the onset of (3) at $h\nu \approx 1.85$ eV. The broad absorptions connected with transitions (2) and (3) are seen in curve 1 of

† It was verified experimentally that the intensity of the absorption lines due to Ni^{2+}_{Ga} at 0.852 and 1.41 eV [10] have the same spectral dependence as the ZPL at 1.232 eV shown in figures 4 and 9.

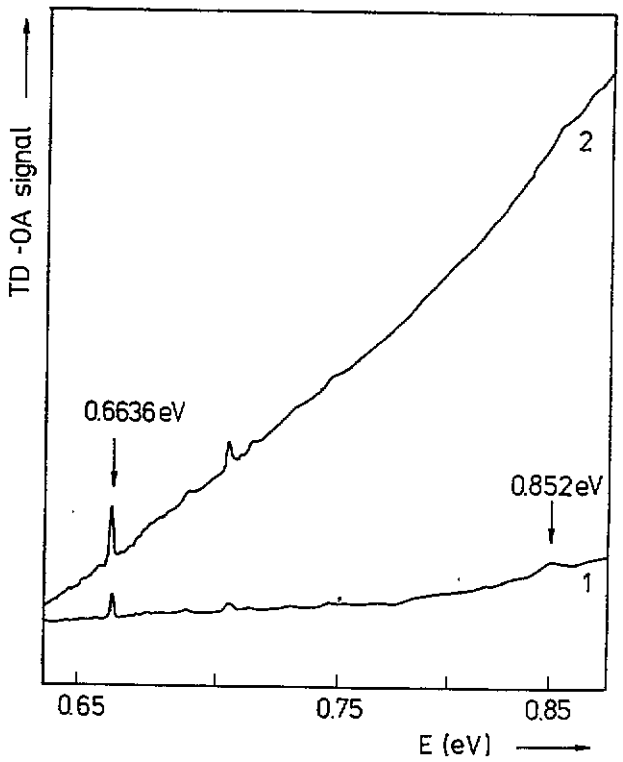

Figure 8. The TD-OA spectra of GaP:Ni:S (sample M1) measured at $T = 1.7$ K in the region of the $^2T_2 \rightarrow {}^2E$ transition of Ni^+_{Ga}: curve 1, after cooling in the dark; curve 2, after illumination with $h\nu_{exc} = 2.15$ eV. Additionally the line at 0.852 eV due to the $^3T_1 \rightarrow {}^3T_2$ transition of Ni^{2+}_{Ga} [10] is seen.

figure 1. The fourth photoionization processes indicated in figure 11,

$$Ni^+_{Ga} + h\nu \rightarrow Ni^{2+}_{Ga} + e_{cb} \tag{4}$$

cannot occur in p-type GaP:Ni because no Ni^+_{Ga} exists.

From figures 4 and 5 it can be ascertained that process (2) dominates, with its onset at approximately 1.4 eV. The holes in the valence band ($hole_{vb}$) created by (2) are captured by other Ni^{2+} ions forming Ni^{3+}, so that

$$Ni^{2+}_{Ga} + hole_{vb} \rightarrow Ni^{3+}_{Ga}. \tag{5}$$

Therefore processes (2) and (5) together explain the measured increase in Ni^{3+} and Ni^+ accompanied by the decrease in Ni^{2+} for $h\nu_{exp} > 1.4$ eV. Thus the photoinduced recharging following from (2) and (5) is given by

$$2Ni^{2+}_{Ga} + h\nu \rightarrow Ni^+_{Ga} + Ni^{3+}_{Ga}. \tag{6}$$

The weak increase in Ni^{3+}_{Ga} for illumination energies 0.85 eV $< h\nu_{exc} < 1.4$ eV can be explained by the process

$$Fe^{3+}_{Ga} + h\nu \rightarrow Fe^{2+}_{Ga} + hole \tag{7}$$

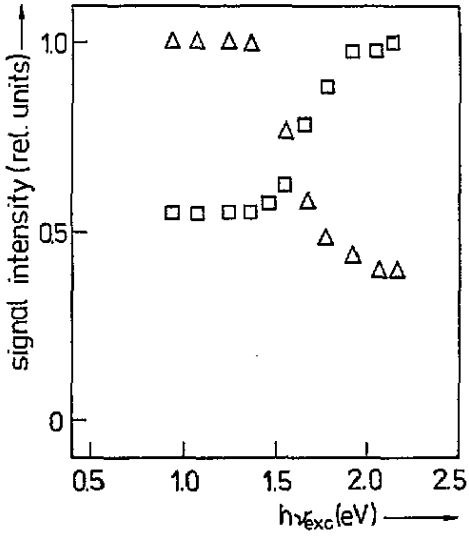

Figure 9. Dependence of the photoinduced changes on illumination energy $h\nu_{exc}$ of GaP:Ni:S (sample M1) measured at $T = 1.7$ K by TD-OA (cf figures 7 and 8): open triangles, intensity of the ZPL at 1.232 eV of the $^3T_1(F) \rightarrow {}^3T_1(P)$ transition of Ni^{2+}_{Ga}; open squares, intensity of the ZPL at 0.6636 eV of the $^2T_2 \rightarrow {}^2E$ transition of Ni^{+}_{Ga}.

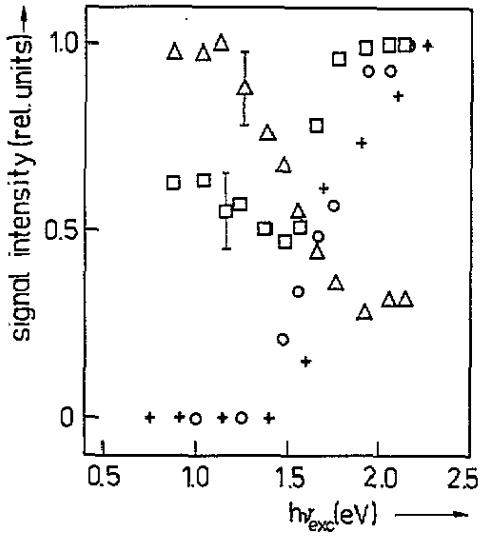

Figure 10. Dependence of the photoinduced changes on illumination energy $h\nu_{exc}$ of GaP:Ni:S (sample M1). TD-EPR signal intensities measured at $T = 4$ K for B along ⟨111⟩: open circles, Ni^{3+}_{Ga}; open squares, Ni^{+}_{Ga}; open triangles, Ni^{2+}. The conventional EPR signal (+) intensity of Ni^{3+}_{Ga} is measured at $T = 20$ K.

which together with (5) creates Ni^{3+}. The residual impurity Fe has its first acceptor level $Fe^{2+}_{Ga}/Fe^{3+}_{Ga}$ at $E_v + 0.82$ eV so that the measured onset for (7) coincides with this level position. The absence of any detectable creation of Ni^{+}_{Ga} for $h\nu_{exc} < 1.4$ eV (see

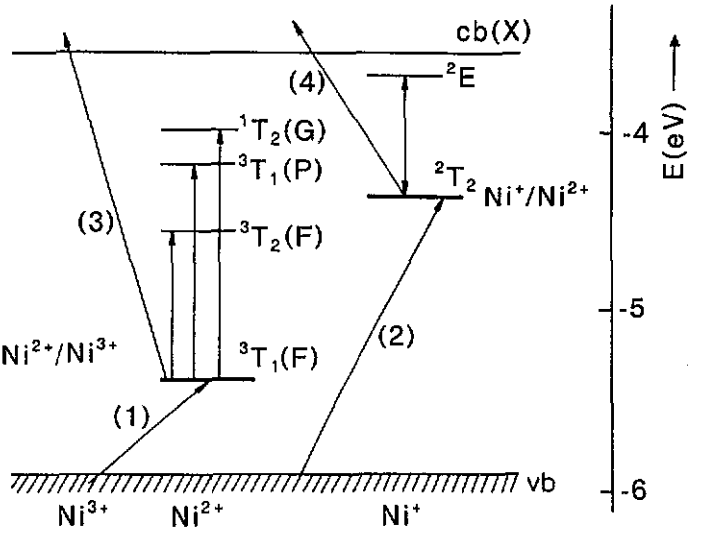

Figure 11. Energy level diagram of Ni_{Ga} in GaP. The energy scale is related to the vacuum level. The vertical arrows indicate the internal transitions of Ni^{2+}_{Ga} and Ni^{+}_{Ga} monitored by optical absorption. The band ↔ impurity photoionization transitions (1) to (4) are those described to the text.

figure 5) supports this interpretation together with the strong decrease in the Fe^{3+}_{Ga} EPR signal measured for $0.85 \leqslant h\nu_{exc} \leqslant 1.4$ eV. It is not yet possible to account for the slight increase in Ni^{2+} in this region of $h\nu_{exc}$. It should be mentioned that this increase observed in p-type GaP:Ni samples is much more pronounced for the TD-EPR signals than for the OA lines. A possible explanation is that TD-EPR is sensitive to photoinduced strains.

After Ni^+ and Ni^{3+} have been created with $h\nu_{exc} > 1.4$ eV according to (6), the result of this recharging process can be reversed optically by illumination into the photoionization absorption of the created Ni^{3+} (see curve 2 of figure 1). A $hole_{vb}$ is created according to (1) in the region $0.55 < h\nu_b < 1.4$ eV and this is subsequently captured by the photoinduced Ni^{+}_{Ga}:

$$Ni^{+}_{Ga} + hole_{vb} \rightarrow Ni^{2+} \tag{8}$$

until the original state is restored. ($h\nu_b$ is the bleaching quantum.) This bleaching process has also been monitored by observing the OA and paramagnetic resonances of Ni^+, Ni^{2+} and Ni^{3+}.

In n-type GaP:Ni:S M1 samples, the Fermi level is pinned by the Ni^{+}_{Ga}/Ni^{2+}_{Ga} level at about $E_c - 0.9$ eV. This means that no Ni^{3+}_{Ga} is present but only Ni^{+}_{Ga} and Ni^{2+}_{Ga}. Thus the possible photoionization transitions involving Ni_{Ga} are processes (2), (3) and (4). Despite this difference, the main photoinduced recharging processes are the same as in the p-type GaP:Ni samples. Figures 9 and 10 show that recharging takes place for $h\nu_{exc} > 1.4$ eV and therefore process (2) is responsible for increasing the Ni^+ content and creating $hole_{vb}$ which are then captured according to (5), creating Ni^{3+}_{Ga}. Both processes are connected with a decrease in the Ni^{2+}_{Ga} content according to (6); this is also evident from figures 9 and 10. This is supported by the second detected hole capture process

$$Fe^{2+}_{Ga} + hole_{vb} \rightarrow Fe^{3+}_{Ga} \tag{9}$$

which shows by monitoring the Fe^{3+}_{Ga} signal with the same spectral dependence on $h\nu_{exc}$ as process (5). As already discussed in connection with figures 4 and 5, the spectral dependence caused by process (2) and seen in figures 9 and 10 is quite close to that of the optical cross section $\sigma_p^\circ(h\nu)$ corresponding to (2) at $T = 95$ K by photocapacitance experiments (cf figure 1 in [4]).

Although a considerable amount of Ni^+_{Ga} is present, process (4) is clearly not effective because the content of the stable traps for electrons excited into the conduction band is too small. The mechanism for the optical restoration of the photoinduced recharging is also the same as in p-type GaP:Ni (i.e. processes (1) and (8)).

Summarizing the analysis of the photoinduced recharging processes involving Ni_{Ga}, we can conclude that the experiments can be consistently explained by the recharging process (6). Therefore, the assignment of the TD-EPR lines to Ni^{2+}_{Ga} would to be correct. As the spectroscopic features of the Ni^{3+}_{Ga} and Ni^+_{Ga} created by illumination at low temperatures are those of isolated Ni_{Ga}, the Ni^{2+}_{Ga} from which they originate must also be isolated. The only remaining problem is the explanation of the observed increase in the Ni^{2+} signals (together with those belonging to Ni^{3+} and Ni^+) when $h\nu_{exc}$ is less than approximately 1.4 eV.

5. The orthorhombic Jahn–Teller model for Ni^{2+}_{Ga}

5.1. The experimental TD-EPR isofrequency curves

From the photocharging experiments, and taking into account that they are due to centres which are very strongly coupled to the lattice, new peaks in the TD-EPR spectra have been assigned to the isolated Ni^{2+}_{Ga} ion. To verify this assignment, further TD-EPR experiments have been undertaken at $T = 4$ K in which the direction of the magnetic field $\boldsymbol{B}$ was varied in the (110) plane at a fixed quantum frequency of 9.3 GHz. From these data, isofrequency curves for Ni^{2+}_{Ga} can be constructed. A typical set of results is shown in figure 12. In this figure all of the other resonance peaks (e.g. those shown in figure 3) have been removed for clarity. (It is very important to emphasize that all of the resonances shown in figure 12 are very clearly correlated with each other and thus all of them come from the same centre. Also none of the experimental points excluded from this figure come from this centre.) On examination of these curves, it is seen that they display orthorhombic symmetry as, for example, there are at least three separate components of which two different pairs coincide for $\boldsymbol{B}$ along ⟨001⟩ and ⟨110⟩. In one set of results, it was found that one of these curves was split into two, showing that it can be due to two different sites. (We refer to this result later when we attribute this small splitting in this particular experiment to the fact that the magnetic field was not rotated in the exact (110) plane.)

5.2. The model

The model which we propose to account for these results follows closely that used very recently by Parker *et al* [18] for the GaAs:Cr^{3+} system. This orthorhombic Jahn–Teller model was based on the earlier work of Dunn and Bates [20]. We do not think that the model proposed some time ago by Liro and Baranowski [9] for Ni^{2+}_{Ga} in GaP to account for their uniaxial stress and Zeeman experiments in optical studies is appropriate. Their model of the $^3T_1(F)$ ground state assumes that it is split sufficiently by first-order spin–orbit coupling that an A_1 singlet lies lowest and that

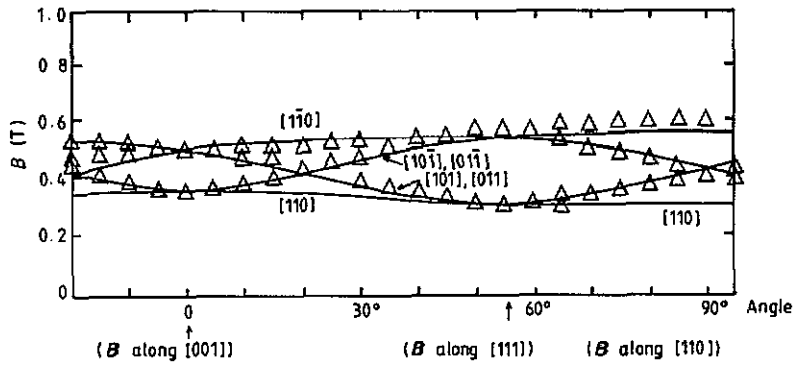

Figure 12. Angular dependence of the resonant magnetic field positions of the Ni^{2+}_{Ga} resonances measured by TD-EPR at $T = 4$ K with $\nu = 9.3$ GHz (open triangles, experimental points; full curve, theory). The symmetries of the strain-stabilized orthorhombic sites which produce the isofrequency curves are also given in the form [110] etc.

it is well separated from the remaining energy levels. The observed structure in the optical spectra was explained entirely by splittings within the $^3T_1(P)$ excited state. We believe that the absolute ground state cannot be an isolated orbital singlet for a number of reasons:

(i) The phonon-scattering experiments [11, 12] clearly show that strong scattering from Ni^{2+}_{Ga} occurs and that the results are consistent with an orthorhombic symmetry associated with a dynamic orthorhombic Jahn–Teller effect.

(ii) Our own TD-EPR experiments show that the Ni^{2+} resonances are intense relative to other ion impurities in GaP of similar nominal concentrations and thus that the ion responsible is very strongly coupled to the surrounding lattice. Moreover, as in the case of Cr^{3+} in GaAs [18], the relative intensities of these peaks vary with the sample whereas the resonance field is unchanged. In one sample in particular, the strain is probably caused by temperature variations.

(iii) The angular dependences of the isofrequency curves display orthorhombic symmetry as stated earlier.

(iv) All other ions with T_1 states in III–V semiconductors show very strong coupling to the surrounding lattice and undergo strong Jahn–Teller effects as a result (e.g. [11, 12, 21]). In addition, it appears that coupling to both e- and t_2-modes occurs with the t_2-mode coupling significant and rarely less than the e-mode coupling.

As a result, we will assume from the outset that strong Jahn–Teller effects operate in the $^3T_1$ ground state, that the coupling to the t_2- and e-modes is approximately the same and that the orthorhombic nature of the spectrum is generated by resonances from strain-stabilized sites of isolated Ni^{2+} ions [20]. This arises when resonances from sites with different strain magnitudes occur at the same magnetic field. This condition is met when the separation of two energy levels between which the transition occurs remains constant over large ranges of the strain as the magnetic field is increased.

The effective Hamiltonian within the $^3T_1$ ($l = 1$) ground state can be written in the form [17]:

$$\mathcal{H}_{\text{eff}} = \mathcal{H}_{\text{SO}} + \mathcal{H}_B + \mathcal{H}_{\text{strain}} \tag{10}$$

where the spin–orbit coupling is written as

$$\mathcal{H}_{SO} = a(\boldsymbol{l}\cdot\boldsymbol{S}) + b(\boldsymbol{l}\cdot\boldsymbol{S})^2 + c(E^l_\theta E^S_\theta + E^l_\epsilon E^S_\epsilon) \tag{11}$$

the Zeeman term is approximated to

$$\mathcal{H}_B = \mu_B\{[\boldsymbol{B}\cdot(-\tfrac{3}{2}\gamma\boldsymbol{l} + 2\boldsymbol{S}) + 2c[(\boldsymbol{B}\cdot\boldsymbol{S}) + (E^l_\theta E^{BS}_\theta + E^l_\epsilon E^{BS}_\epsilon)] + b[(\boldsymbol{l}\cdot\boldsymbol{S})(\boldsymbol{l}\cdot\boldsymbol{B}) + (\boldsymbol{l}\cdot\boldsymbol{B})(\boldsymbol{l}\cdot\boldsymbol{S})]\} \tag{12}$$

and the strain term is written as

$$\mathcal{H}_{strain} = V(E^l_\theta \pm kT_{xy}) \tag{13}$$

for sites with axes [110] and [$\bar{1}$10] denoted by '+' and '−' respectively. A cyclic interchange of the symmetry labels in (13) generates the Hamiltonians for the remaining sites. Previously $E^l_\theta, E^l_\epsilon, T_{xy}$ etc were orbital operators where

$$E^l_\theta = \tfrac{1}{2}[3l_z^2 - 2] \qquad E^l_\epsilon = \tfrac{1}{4}\sqrt{3}[l_+^2 + l_-^2] \qquad T_{xy} = l_x l_y + l_y l_x. \tag{14}$$

E^S_θ is also equivalent to E^l_θ with l replaced by S etc.

Equations (12) and (13) contain several parameters which need to be determined. The parameters a, b, c and γ arise from the Jahn–Teller effect and V and k from the strain. However, a simplification may be made by approximating a to $[-(\frac{3}{2})\gamma\lambda]$ where λ ($= -300$ cm^{-1}) is the spin–orbit coupling constant; the factor of $(-\frac{3}{2})$ is the isomorphic coupling constant (which also appeared in (12)).

As the ion–lattice coupling is strong, a is small so that $\mathcal{H}_{strain}$ is the largest term in $\mathcal{H}_{eff}$. Acting alone, $\mathcal{H}_{strain}$ splits $^3T_1$ into three spin triplets which are generally separated from each other. The spin degeneracies associated with each of the orbital states are then removed by the second-order spin–orbit coupling terms (in b and c) within $\mathcal{H}_{SO}$. The EPR can then arise from the Zeeman splitting of the three levels which are lowest in energy.

Insufficient data are available to determine the values of the parameters by analytical methods and thus computing methods have been employed. Three stages in the fitting routine were identified. First, V was taken to be $+100$ cm^{-1} to satisfy the strain-stabilized condition. Second, arbitrary values were taken for the unknown parameters (consistent with reasonable physical expectation) and, third, site labels were attached to the isofrequency curves in order to reflect the observed symmetry and degeneracies. The 9×9 matrix of $\mathcal{H}_{eff}$ was diagonalized by computer. A standard sum of squares fitting procedure was employed to obtain the best set of parameters. All the experimental points such as those shown in figure 12 were used. As usual in such problems, the procedure was not straightforward as the assignment of site symmetries to the various isofrequency curves was very much affected by the values chosen for the parameters.

After a considerable amount of computing, which included checks to ensure that the strain stabilization condition was satisfied, it was found that the experimental isofrequency curves were a good fit to the theory outlined above for the 2–3 transition with:

$$a = 0.2 \text{ cm}^{-1}$$

$$b = -0.093 \text{ cm}^{-1}$$

$$c = -0.032 \text{ cm}^{-1}$$

and

$$k = 0.75. \tag{15}$$

(The labels 2 and 3 refer to the two upper levels of the lowest spin triplet.) The theoretical isofrequency curves generated by these parameters are also shown in figure 12. The figure includes the labelling of the various sites. Further sets of programmes were run taking $V = -100$ cm^{-1}. No fits at all were obtained with V negative and so the parameter values given in (15) are assumed to be the correct set.

With these parameter values, the energy levels themselves consisted of a very close ground set (within about 1 cm^{-1}) of six levels plus an upper set of three equally close levels much higher in energy. Thus the 2–3 transition does not suffer any significant depopulation. (It is found that the parameter values are such that the two lowest spin triplets are very close in energy.)

It is clear that experimental points associated with the 2–3 transition from [110] sites are absent in figure 12. The 1–2 transitions also appear to be missing as well. The first experimental data points are believed to be absent because the EPR transition probability is very small or zero. (It is usual for some TD-EPR resonances to be absent for this reason.) They can then be obscured by resonances from ions other than Ni^{2+}_{Ga} ions. Calculations have shown that, with these parameter values, the 1–2 isofrequency curves from strain-stabilized sites have a much more rapid variation with the magnetic field angle than those from the 2–3 transitions and are thus very difficult to separate from the many non-Ni^{2+}_{Ga} resonances particularly if the transition probability is not high. Again, this is a familiar situation in TD-EPR experiments.

As mentioned earlier, one experiment indicated a small splitting of the points which are labelled with sites [011] and [101]. We suppose that this is due to a small misorientation of the (110) plane in which the magnetic field is rotated in that experiment. This in turn confirms that the corresponding isofrequency curve without any misorientation consists of two degenerate resonances from two sites.

5.3. Comments

The results (15) are consistent with a very strong Jahn–Teller effect as the first-order reduction factor γ, which has a value of 4×10^{-4}, is very small. In principle, it should be possible to obtain values for the fundamental parameters from (15) and the expressions for them given in Dunn and Bates [20, equation (4.18)]. Unfortunately the data are insufficient to do so. Moreover, further more accurate calculations of the reduction factors are currently in progress [23] and these will replace the simple forms given in Dunn and Bates [20]. They also show that certain numerical factors were omitted in plotting some of the original graphs.

6. Conclusions

It is very difficult to attempt to correlate the model proposed earlier for our TD-EPR data with that needed to explain the optical data of Liro and Baranowski [9] because in the optical experiments the ions responsible for the ZPL peaks are likely to be those with zero strain. In addition, a detailed analysis of these optical data requires a model for the excited state. This is beyond the scope of the present work.

The work described in this paper can be divided into two distinct parts but with a strong connection between them. One series of measurements describes photoinduced recharging experiments on GaP:Ni samples with different Fermi level positions. The analysis of the dependence of the intensities of the Ni-related signals on the energy of illumination is discussed in detail. It clearly suggests that the centre responsible for the new TD-EPR resonances, which are very strongly coupled to the lattice, is Ni^{2+}_{Ga}. The second set of measurements and the accompanying theory consists of a detailed study of the angular dependence of these new peaks in the TD-EPR experiments which were clearly related. The good fit between theory and experiment led us to attribute the lines to the Ni^{2+}_{Ga} ion. It also demonstrated that the ion is strongly coupled to both e- and t_2-modes. As in the case of Cr^{3+} ions in GaAs, resonances were shown to arise from strain-stabilized sites of orthorhombic symmetry in accordance with the results of phonon-scattering experiments. (There was no evidence of any significant EPR from sites of zero strain.)

Acknowledgments

We wish to thank Dr J L Dunn and Professor B Clerjaud for many helpful discussions. We also gratefully acknowledge the Royal Society, the (former) Academy of Sciences of the DDR, and the EC for supporting this collaborative programme. One of us (MSGA-A) wishes to thank the Government of Saudi Arabia for a research grant.

References

[1] Clerjaud B 1985 *J. Phys. C: Solid State Phys.* **18** 3615
[2] Peaker A R, Kaufmann U, Wang Z G, Worner R, Hamilton B and Grimmeiss H G 1984 *J. Phys. C: Solid State Phys.* **17** 6161
[3] Abagian S A, Ivanov G A and Koroleva G A 1976 *Fiz. Tekh. Poluprov.* **10** 1773 (Engl. Transl. 1976 *Sov. Phys.-Semicond.* **10** 1056)
[4] Yang X Z, Samuelson L and Grimmeiss H G 1984 *J. Phys. C: Solid State Phys.* **17** 6521
[5] Szawelska H R, Mudhar P S and Allen J W 1984 *J. Phys. C: Solid State Phys.* **17** 2981
[6] Kaufmann U and Schneider J 1978 *Solid State Commun.* **25** 1113
[7] Ueda Y, Niklas J R, Spaeth J M, Kaufmann U and Schneider J 1983 *Solid State Commun.* **46** 127
[8] Baranowski J M, Allen J W and Pearson G L 1968 *Phys. Rev.* **167** 758
[9] Liro Z and Baranowski J M 1982 *J. Phys. C: Solid State Phys.* **15** 4599
[10] Jezewski M, Liro Z and Baranowski J M 1987 *J. Phys. C: Solid State Phys.* **20** 311
[11] Sahraoui-Tahar M, Salce B, Challis L J, Butler N, Ulrici W and Cockayne B 1989 *J. Phys.: Condens. Matter* **1** 9313
[12] Challis L J, Salce B, Butler N, Sahraoui-Tahar M and Ulrici W 1989 *J. Phys.: Condens. Matter* **1** 7277
[13] Kaufmann U, Koschel W H, Schneider J and Weber J 1979 *Phys. Rev.* B **19** 3343
[14] Hayes W, Ryan J F, West C L and Dean P J 1979 *J. Phys. C: Solid State Phys.* **12** L815
[15] Ennen H, Kaufmann U and Schneider J 1981 *Appl. Phys. Lett.* **38** 355
[16] Ennen H and Kaufmann U 1980 *J. Appl. Phys* **51** 1615
[17] Nakib A, Houbloss S, Vasson A and Vasson A M 1988 *J. Phys. D: Appl. Phys.* **21** 478
[18] Parker L W, Bates C A, Dunn J L, Vasson A and Vasson A M 1990 *J. Phys.: Condens. Matter* **2** 2841
[19] Yang X Z, Grimmeiss H G and Samuelson L 1983 *Solid State Commun.* **48** 427
[20] Dunn J L and Bates C A 1989 *J. Phys.: Condens. Matter* **1** 2617
[21] Bates C A, Dunn J L and Ulrici W 1990 *J. Phys.: Condens. Matter* **2** 607
[22] Dunn J L and Bates C A 1988 *J. Phys. C: Solid State Phys.* **21** 2495
[23] Hallam L, Dunn J L and Bates C A *J. Phys.: Condens. Matter* to be submitted